Nanoscale

Accepted Manuscript

This article can be cited before page numbers have been issued, to do this please use: K. Liu, F. Wang, K. Xu, T. A. Shifa, Z. Cheng, X. Zhan and J. He, *Nanoscale*, 2016, DOI: 10.1039/C5NR07735D.

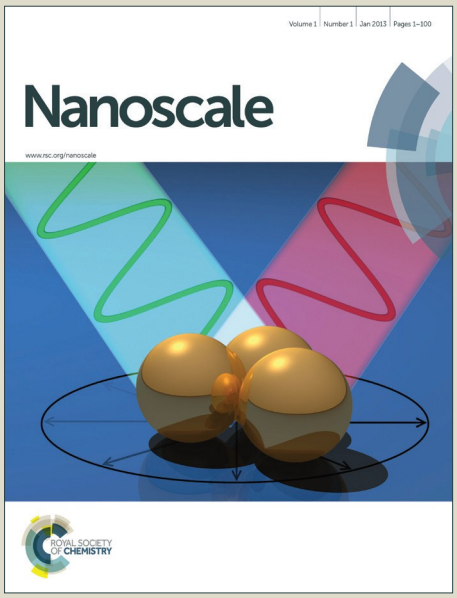

This is an *Accepted Manuscript*, which has been through the Royal Society of Chemistry peer review process and has been accepted for publication.

Accepted Manuscripts are published online shortly after acceptance, before technical editing, formatting and proof reading. Using this free service, authors can make their results available to the community, in citable form, before we publish the edited article. We will replace this *Accepted Manuscript* with the edited and formatted *Advance Article* as soon as it is available.

You can find more information about *Accepted Manuscripts* in the Information for Authors.

Please note that technical editing may introduce minor changes to the text and/or graphics, which may alter content. The journal's standard Terms & Conditions and the Ethical guidelines still apply. In no event shall the Royal Society of Chemistry be held responsible for any errors or omissions in this *Accepted Manuscript* or any consequences arising from the use of any information it contains.

ROYAL SOCIETY OF CHEMISTRY

www.rsc.org/nanoscale

View Article Online
DOI: 10.1039/C5NR07735D

Nanoscale

ARTICLE

$CoS_{2x}Se_{2(1-x)}$ Nanowire Array: An Efficient Ternary Electrocatalyst for Hydrogen Evolution Reaction

Received 00th January 20xx,
Accepted 00th January 20xx

DOI: 10.1039/x0xx00000x

www.rsc.org/

Kaili Liu[a,b,c†], Fengmei Wang[a,b†], Kai Xu[a,b], Tofik Ahmed Shifa[a,b], Zhongzhou Cheng[a], Xueying Zhan[a] and Jun He[a]*

Binary transition metal dichalcogenides (TMDs) have emerged as efficient catalysts for hydrogen evolution reaction (HER). Co-based TMDs, such as CoS_2 and $CoSe_2$, demonstrate promising HER performance due to their intrinsic metallic nature. Recently, the ternary electrocatalysts are widely acknowledged for their prominent efficiency as compared to their binary counterparts due to increased active sites caused by the incorporation of different atoms. Herein, we successfully grow the ternary $CoS_{2x}Se_{2(1-x)}$ ($x \approx 0.67$) nanowires (NWs) on flexible carbon fiber. As a superior electrocatalyst, ternary $CoS_{2x}Se_{2(1-x)}$ NWs arrays demonstrate excellent catalytic activity for electrochemical hydrogen evolution in acidic media, achieving current densities of 10 mA/cm^2 and 100 mA/cm^2 at overpotentials of 129.5 mV and 174 mV, respectively. Notably, the high stability of $CoS_{2x}Se_{2(1-x)}$ NWs suggests that the ternary $CoS_{2x}Se_{2(1-x)}$ NWs to be a scalable catalyst for electrochemical hydrogen evolution.

Introduction

In the quest for renewable and spotless energy, hydrogen has been broadly identified as a potential candidate due to its high energy capacity and environmental friendliness.[1] The production of H_2 has, therefore, drawn a widespread attention.[2-10] To this end, direct reduction of water molecule is promising, yet it is underdeveloped. The critical step in electrolyzing water is hydrogen evolution reaction (HER, $2H^+ + 2e^- \rightarrow H_2$) demanding the innovation of non-noble metal electrocatalysts to achieve high current density at low overpotential.[11] Therefore, exploration of economically viable, highly active, acid-stable HER electrocatalyst is exceedingly desirable.[12] Plethora of materials such as transition metal carbides,[13, 14] metal alloys[15, 16] and metal oxides[17] have been hitherto investigated as catalysts for the electrochemical HER. However, as compared to Pt, those catalysts still suffer from inferior catalytic activity in acidic solutions and the performance of which is still in the exploration stage. Owing to their intriguing chemical and electronic properties, TMDs such as MoS_2,[18-21] WS_2[10, 22, 23] and CoS_2[24] are emerging as a class of key prospects for HER electrocatalysts. Among them, Co based materials of various morphologies such as $CoSe_2$ nanoparticles,[25] $CoSe_2$ film[26] and CoS_2[27] nanowires have been found to demonstrate impressive HER performances due to their intrinsic metallic nature. Moreover, composites of $CoSe_2$ nanobelts with Mn_3O_4 nanopartcile,[28] MoS_2 nanosheet[29] and Ni/NiO nanoparticle[30] have been reported to reveal synergism leading to enhanced electrocatalytic[28-30] performance as compared to their single component counterparts. Notably, the component controllably fabricated ternary systems as in our previous report[31] of $WS_{2(1-x)}Se_{2x}$ nanotube, where in it the number of active sites increased, illustrates the evolution of H_2 at remarkably low overpotential, presently. Gong, et al.[32] extended this framework for $MoS_{2(1-x)}Se_{2x}$ alloy nanoflakes showing the fact that neither of the binary systems performs as good as the ternary one. It is, thus, believed that optimizing the components of S and Se atoms can modify the chemical and physical properties in the ternary system. Inspired by this and speculating the impressive records of Co based TMDs reported so far, we anticipate that the ternary $CoS_{2x}Se_{2(1-x)}$ could be prominent electrocatalyst for HER.

Herein, we report a two-step process for synthesizing $CoS_{2x}Se_{2(1-x)}$ nanowire arrays on carbon fiber ($CoS_{2x}Se_{2(1-x)}$ NWs) meant for electrocatalyst in HER. Accordingly, the self-supported $CoS_{2x}Se_{2(1-x)}$ NWs electrode exhibits excellent electrocatalytic activity evidenced from the achieved current density of 10 mA/cm^2 and 100 mA/cm^2 at overpotential of only 129.5 mV and 174 mV respectively. Furthermore, accelerated disintegration test reveals the exceptional stability of the electrode as its activity endured even after 1000 cycles of cyclic voltammetry (CV) run. Given the very small record of overpotential required for generation of remarkable current density and the long term stability, our novel material represents scalable electrocatalyst for water splitting.

[a] CAS Key Laboratory of Nanosystem and Hierarchical Fabrication, National Center for Nanoscience and Technology, 100190, Beijing, P. R. China.
[b] University of Chinese Academy of Science, No.19AYuquan Road, Beijing 100049, China.
[c] Sino-Danish Center for Education and Research, Beijing, 100190, China.
† These authors contributed equally to this work.

Electronic Supplementary Information (ESI) available: TEM images and CV curves of CoS_2, CoSe2 and $CoS_{2x}Se_{2(1-x)}$ NWs. See DOI: 10.1039/x0xx00000x

View Article Online
DOI: 10.1039/C5NR07735D

Experimental section

Synthesis of CoO NWs

The CoO NWs were grown on carbon fibers (CFs) by a method that we have recently reported.[33] In detail, the CFs were first ultrasonically washed by a mixture of acetone, ethanol and ultrapure water, and then dried at 60 °C. Subsequently, the dried CFs were soaked in the solution, containing 1.90 g $CoCl_2 \cdot 6H_2O$, 2.424 g $CO(NH_2)_2$ and 40mL ethanol, for 10 min. The soaked CFs were calcined under a flow of argon at 450 °C for 4 h to form a seed layer on CFs. Second, the mixture of 1.90 g $CoCl_2 \cdot 6H_2O$, 2.424 g $CO(NH_2)_2$ and 40 mL ultrapure water was transferred into a 50 mL Teflon-lined stainless steel autoclave, followed by putting one piece of the seeded CFs in the solution. The autoclave was then heated in an electrical oven at 90 °C for 4 h to synthesize $Co(OH)_2$ NWs. Eventually, the CoO NWs were formed by annealing the $Co(OH)_2$ NWs under a 100 sccm argon flow at 500 °C for 4 h.

Synthesis of $CoS_{2x}Se_{2(1-x)}$ NWs

The second step is conducted in a horizontal quartz tube furnace to convert the CoO NWs into $CoS_{2x}Se_{2(1-x)}$ NWs. The CFs covered by CoO NWs was placed at the downstream side of the tube furnace and 0.5 g mixed powder with different mass ratio (Se: S) was placed at the upstream side of the tube furnace. The distance between them is 22 cm. To create an oxygen-free environment, the tube furnace was flushed three times under a 100 sccm Ar flow. After flushed with Ar, the part of the CoO NWs was quickly heated to 450 °C in 20 min and reacted for 95 min. Meanwhile, the zone of sulfur and selenium powder was fast heated to 125 °C in 20 min and then increase to 275 °C in 5 min, and the reaction temperature was slowly increased to 300 °C within 90 min. During the whole process, the flow of Ar was kept at a rate of 100 sccm. For comparison, the CoS_2 and $CoSe_2$ NWs were also synthesized through similar method (see supporting information).

Characterizations

The characterizations of CoO NWs and $CoS_{2x}Se_{2(1-x)}$ NWs were carried out by field emission scanning electron microscopy (FESEM, Hitach S-4800), transmission electron microscopy (TecnaiF20), X-ray diffraction (XRD) (Philips X'Pert Pro Super) on an X-ray powder diffractometer with Cu Kα radiation (λ = 1.5418 Å) and X-ray photoelectron spectroscopy (ESCALAB250Xi).

Electrochemical measurements

Electrochemical measurements were performed in a typical three-electrode system in 0.5 M H_2SO_4 (N_2 saturated) at an electrochemical station (CHI 660D). In all measurements, the potentials were calibrated to a reversible hydrogen electrode (RHE). The CF, onto which $CoS_{2x}Se_{2(1-x)}$ NWs grown on it, served as a working electrode whereas a platinum wire and a saturated calomel electrode as the counter electrode and reference electrode, respectively. Linear sweep voltammetry measurements were conducted in 80 ml of a 0.5 M H_2SO_4 solution with a scan rate of 2 mV/s. Electrochemical impedance spectroscopy was performed when the working electrode was biased at a constant -0.118V vs.RHE with the frequency ranging from 1 MHz to 0.001 Hz with an amplitude of 10 mV. Cyclic voltammetry experiments were carried out from 0 to +0.1 V vs. RHE with different scan rates (20-200 mV/s) to estimate the double-layer capacitance.

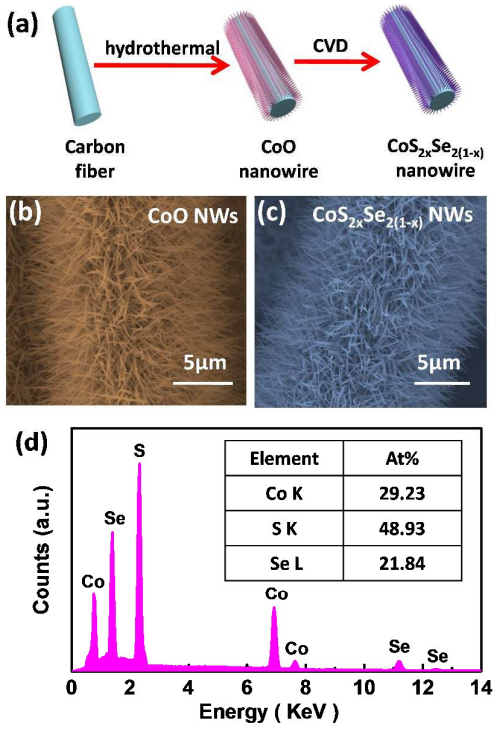

Fig. 1 (a) Schematic diagram of the preparation of $CoS_{2x}Se_{2(1-x)}$ nanowires on carbon fiber ($CoS_{2x}Se_{2(1-x)}$ NWs). SEM images of CoO NWs (b) and $CoS_{2x}Se_{2(1-x)}$ NWs (c). (d) EDX spectrum of $CoS_{2x}Se_{2(1-x)}$ NWs.

Results and discussion

Following our recent report[33] on CoO NWs, we employed a facile chemical vapor deposition (CVD) method for further converting them to $CoS_{2x}Se_{2(1-x)}$ through simultaneous sulfurization and selenization reaction. Fig. 1a depicts the schematic diagram of the synthetic process. The low-magnification scanning electron microscopy (SEM) images of CoO NWs and $CoS_{2x}Se_{2(1-x)}$ NWs are revealed in Fig. 1b and c. It is apparent that, the NW morphology of CoO remains unchanged after successfully converting to $CoS_{2x}Se_{2(1-x)}$. The necklace-like ternary NWs expose large accessible area wherein each NW consists of nanoparticles with size of 200 nm. Meanwhile, the similar morphology and size of CoS_2 NWs and $CoSe_2$ NWs are demonstrated in Fig. S1a and b. In order to analyze the chemical composition of $CoS_{2x}Se_{2(1-x)}$ NWs, the energy-dispersive X-ray spectroscopy (EDX) spectrum (Fig. 1d) was conducted. As shown in Fig. 1d, the EDX demonstrates the presence of Co, S and Se elements with no discernible O atom confirming the successful conversion of CoO to $CoS_{2x}Se_{2(1-x)}$. Moreover, the inset table of Fig. 1d reveals that the atomic ratio of S: Se is close to 2:1 (x ≈ 0.67). The low-magnification TEM image in Fig. 2a displays the formation of

View Article Online
DOI: 10.1039/C5NR07735D

crystalline $CoS_{2x}Se_{2(1-x)}$ NW with diameter around 200 nm and the length about 4 micrometers (Fig. S1c). Furthermore, the high-resolution TEM (HRTEM) image in Fig. 2b indicates that the interplanar spacing of the crystal lattice in $CoS_{2x}Se_{2(1-x)}$ NWs is ~0.235 nm, which is between that of CoS_2 (0.226 nm) and $CoSe_2$ (0.239 nm), toward [211] crystal orientation. The change of the crystal lattice results from the introduction of Se atoms to the CoS_2. Notably, it is also evident from the scanning TEM (STEM) image and

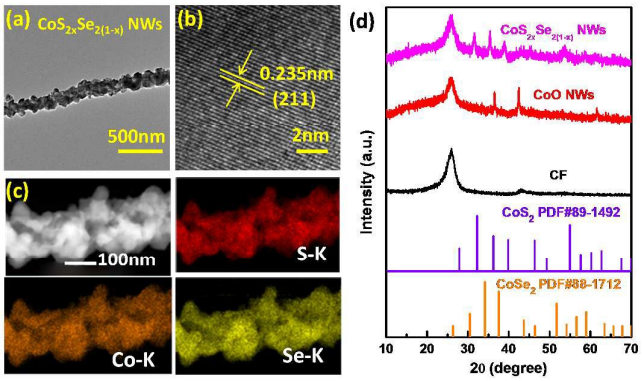

energy-dispersive X-ray (EDX) elemental mapping images (Fig. 2c) that the elements are distributed uniformly in the $CoS_{2x}Se_{2(1-x)}$ NW.

Fig. 2 TEM image (a) and HRTEM image (b) of a $CoS_{2x}Se_{2(1-x)}$ NW. (c) STEM image and EDX elemental mapping of a $CoS_{2x}Se_{2(1-x)}$ NW. (d) XRD patterns of bare CF, CoO NWs and $CoS_{2x}Se_{2(1-x)}$ NWs.

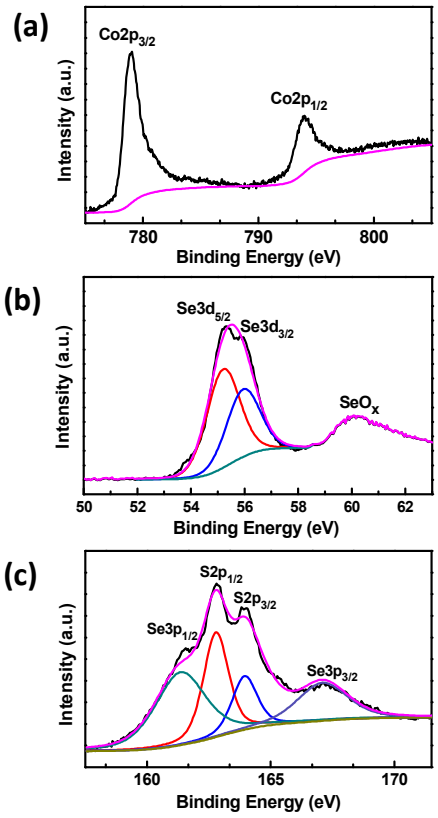

Fig. 3 XPS spectra of (a) Co 2p, (b) Se 3d and (c) S 2p and Se 2p region.

Fig. 2d presents the powder X-ray diffraction (XRD) patterns of bare CF, CoO NWs and $CoS_{2x}Se_{2(1-x)}$ NWs. The observed broadened peak at the angle region of ~25° in all samples is attributed to the diffraction characteristics of CFs. Compared with the XRD pattern of cubic-phased CoO NWs (PDF#74-2391), there is no CoO diffraction peaks in $CoS_{2x}Se_{2(1-x)}$, CoS_2 and $CoSe_2$ NWs (Fig. S2), suggesting the complete conversion of CoO NWs as well as further confirming the previous results. Notably, these synthesized NWs possess cubic pyrite-structured phase. In comparison with CoS_2 (PDF# 89-1492) and $CoSe_2$ (PDF# 88-1712), we also found that all the degree of characteristic diffraction peaks in $CoS_{2x}Se_{2(1-x)}$ shift owing to the different size of selenium atom and sulfur atom. This corroborates the result we obtained from HRTEM. Additionally, X-ray photoelectron spectroscopy (XPS) analysis of $CoS_{2x}Se_{2(1-x)}$ was performed to further investigate the chemical states of cobalt and the chalcogens (Fig. 3a-c and Fig. S3). As shown in Fig. 3a, two peaks corresponding to Co $2p_{3/2}$ and $2p_{1/2}$ are observed. It is noteworthy that the peaks in $CoS_{2x}Se_{2(1-x)}$ sample are located at binding energy of 778.85 eV and 793.94 eV with a slight shift as compared to binary CoS_2 and $CoSe_2$.[25, 27] The peaks of Se $3d_{5/2}$ ($Se3d_{3/2}$) and S $2p_{3/2}$ ($S2p_{1/2}$) are located at 55.2 eV (55.8 eV) and 162.78 eV (163.88 eV) (Fig. 3b), respectively. The oxygen signal depicts the phenomena of surface oxide contamination.[25] Quantitative analysis has been performed for S and Se in the alloy with the S: Se ratios of 2:1, which is consistent with the EDX result.

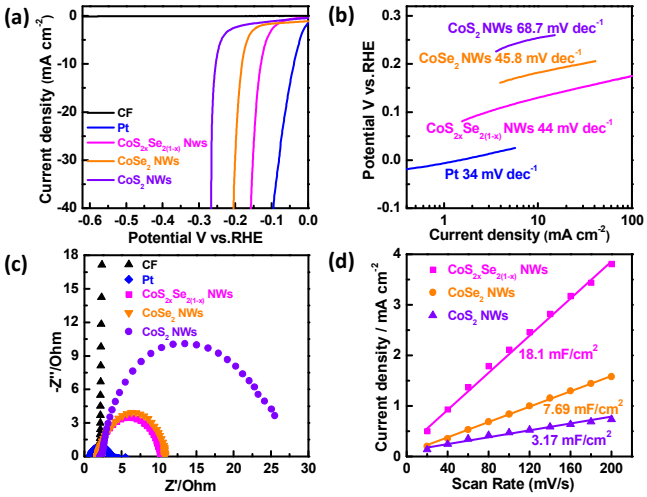

Fig. 4 (a) Polarization curves for bare CF, Pt, CoS_2 NWs, $CoSe_2$ NWs and $CoS_{2x}Se_{2(1-x)}$ NWs. (b) Tafel plots for Pt, CoS_2 NWs, $CoSe_2$ NWs and $CoS_{2x}Se_{2(1-x)}$ NWs. (c) Nyquist plots for bare CF, Pt, CoS_2 NWs, $CoSe_2$ NWs and $CoS_{2x}Se_{2(1-x)}$ NWs carried out under an overpotential of -0.118V (vs. RHE). Inset is the magnified Nyquist plot at high frequency region. (d) Linear fitting of the capacitive currents at 0.05 V vs. RHE of the catalysts vs. scan rates.

The catalytic performances of our samples were investigated in a typical three-electrode configuration with 0.5 M H_2SO_4 electrolyte (N_2 saturated) at room temperature (see experimental section). For

View Article Online
DOI: 10.1039/C5NR07735D

the sake of comparisons, the bare CF, Pt, CoS_2 NWs and $CoSe_2$ NWs electrodes were also checked. All initial data are presented after iR correction for assessing the intrinsic activity of the catalysts.[34] The polarization curves of all samples in Fig. 4a indicates that the catalytic performance of bare CF is very poor, hence, the observed performance is unambiguously attributable to the NWs grown on CF substrate. Compared with CoS_2 NWs (253 mV at 10 mA/cm^2) and $CoSe_2$ NWs (181 mV at 10 mA/cm^2), $CoS_{2x}Se_{2(1-x)}$ NWs grown on CFs exhibits improved electrocatalytic activity. Notably, the HER activity of $CoS_{2x}Se_{2(1-x)}$ NWs ($x \approx 0.67$) show the best HER performance with current densities of 10 mA/cm^2 and 100 mA/cm^2 at overpotentials of 129.5 mV and 174 mV respectively, among all different samples with various atomic ratio (Fig. S4). This property is more superior than some reported results among cobalt-based electrocatalysts.[25, 27, 35] Moreover, the kinetics of CoS_2 NWs, $CoSe_2$ NWs and $CoS_{2x}Se_{2(1-x)}$ NWs under HER condition were investigated by corresponding Tafel plots, extracted from the polarization curve in Fig. 4a. The linear parts of the Tafel plots (Fig. 4b) reveals the low Tafel slope of 44 mV/dec for $CoS_{2x}Se_{2(1-x)}$ NWs. In contrast, CoS_2 NWs and $CoSe_2$ NWs afforded higher Tafel slope of 68.7 and 45.8 mV/dec, respectively. On the one hand, the best HER performance of the ternary $CoS_{2x}Se_{2(1-x)}$ NWs may be due to the optimal electronic structure of the catalyst for hydrogen evolution through incorporating S and Se atoms.[36] For cobalt dichalcogenide, *d*-electron filling in e_g orbitals contributes primarily to the density of states in the conduction band.[37, 38] And the partially filled e_g orbital promotes the excellent electrocatalytic performance. Thus, the superior HER property of $CoS_{2x}Se_{2(1-x)}$ NWs is probably owing to the unique electronic structure. On the other hand, the electrochemically active surface area is another important parameter to characterize the activity of catalysts. Since the active surface area can be determined by the electrochemical double-layer capacitance, C_{dl},[25] the cyclic voltammograms (CV) curves of $CoS_{2x}Se_{2(1-x)}$ NWs, $CoSe_2$ NWs and CoS_2 NWs were obtained between 0 and 0.1 V (vs. RHE) at different scan rates from 20 mV/s to 200 mV/s (Fig. S2a-c). It can be evidenced from Fig. 4d that the C_{dl} of $CoSe_2$ and CoS_2 NWs are 7.69 mF/cm^2 and 3.17 mF/cm^2 respectively, whereas, that of $CoS_{2x}Se_{2(1-x)}$ NWs is 18.1 mF/cm^2, suggesting the sharply increased electrochemically active surface area of ternary $CoS_{2x}Se_{2(1-x)}$ NWs than the binary ones. Herein, the binary and ternary NWs possess the similar morphology, the greatly improved C_{dl} results from the increase of active sites on the ternary $CoS_{2x}Se_{2(1-x)}$ NWs, which is consistent with some reported results.[39]

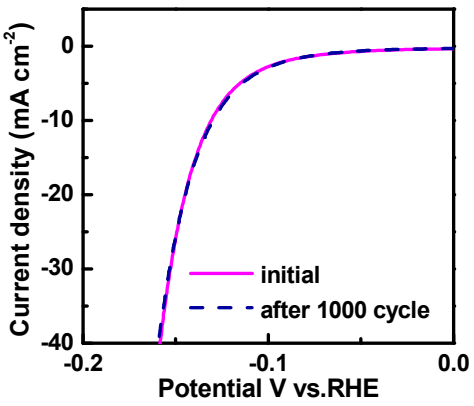

Fig. 5 Stability tests of $CoS_{2x}Se_{2(1-x)}$ NWs with initial polarization curve and the one after 1000 potential cycles.

To study the charge-transfer mechanism of HER on the catalysts, we conducted electrochemical impedance spectroscopy (EIS) measurement (Fig. 4c). The obtained semicircles of EIS indicate that the charge-transfer resistance controls the kinetics at the electrode interface.[40] The charge-transfer resistance (R_{ct}) of $CoS_{2x}Se_{2(1-x)}$ NWs on CF (8.42 Ω), which is much lower than the binary ones (17.13 Ω for CoS_2 and 9.25 Ω for $CoSe_2$), reveals a fast charge transport during the HER process. It is noteworthy that the low series resistance (R_s) value of 1.7 Ω (inset plot of Fig. 4c) suggests the small Ohmic loss in the electrolyte. In general, the superior HER performance of the ternary $CoS_{2x}Se_{2(1-x)}$ NWs in acid media is due to the following points. Firstly, the unique electronic structure of $CoS_{2x}Se_{2(1-x)}$ could facilitate the electrochemical reaction. Secondly, large surface area of necklace-like $CoS_{2x}Se_{2(1-x)}$ NW arrays on CF and much more active sites are exposed after simultaneously introducing the S and Se atoms into the NWs, which is consistent with reported results[39] and confirmed by the increased C_{dl} value in Fig. 4d. Finally, the electrode is obtained without applying the inactive binders through fabricating the $CoS_{2x}Se_{2(1-x)}$ NWs directly on the conductive CFs, avoiding the complicated catalyst preparation techniques. Significantly, the stability of the $CoS_{2x}Se_{2(1-x)}$ NWs was evaluated by conducting potential sweeps between 0 V and -0.44 V vs. RHE for 1000 cycles in the same electrolyte. As is evident from the TEM image (Fig. S6), the morphology of $CoS_{2x}Se_{2(1-x)}$ NWs reserves even after the stability test. Moreover, from Fig. 5, it is obvious that the polarization curve of $CoS_{2x}Se_{2(1-x)}$ NWs after 1000 cycles is similar to the polarization curve of initial $CoS_{2x}Se_{2(1-x)}$ NWs. These results demonstrate the excellent stability of $CoS_{2x}Se_{2(1-x)}$ NWs on the CFs for HER.

Conclusions

In summary, we have successfully fabricated the ternary $CoS_{2x}Se_{2(1-x)}$ NW arrays on carbon fiber via a two-step process. As an earth-abundant and binding-free material, $CoS_{2x}Se_{2(1-x)}$ NWs can be directly used as a stable electrode for hydrogen evolution in the acid media. Compared with binary ones, our ternary sample has much larger active surface area, lower overpotential (129.5 mV at 10 mA/cm^2) and smaller Tafel slope (44 mV/dec). The excellent HER performance and stability reveals that $CoS_{2x}Se_{2(1-x)}$ NWs is an outstanding electrocatalyst. It offers us a promising catalyst for large-scale water-splitting application.

Acknowledgements

This work was supported by the National Natural Science Foundation of China (Nos. 21373065 and 61474033), 973 Program of the Ministry of Science and Technology of China (No. 2012CB934103), Beijing Natural Science Foundation (No. 2144059) and CAS Key Laboratory of Nanosystem and Hierarchical Fabrication. The authors gratefully acknowledges the support of K.C. Wong Education Foundation.

View Article Online
DOI: 10.1039/C5NR07735D

Notes and references

1 J. A. Turner, *Science*, 2004, **305**, 792-794.
2 D. J. Li, U. N. Maiti, J. Lim, D. S. Choi, W. J. Lee, Y. Oh, G. Y. Lee and S. O. Kim, *Nano Lett.*, 2014, **14**, 1228-1233.
3 C. He, X. Wu, J. Shen and P. K. Chu, *Nano Lett.*, 2012, **12**, 1545-1548.
4 D. Wang, Z. Pan, Z. Wu, Z. Wang and Z. Liu, *J. Power Sources*, 2014, **264**, 229-234.
5 S. Bai, C. Wang, M. Deng, M. Gong, Y. Bai, J. Jiang and Y. Xiong, *Angew. Chem. Int. Ed.*, 2014, **53**, 12120-12124.
6 W. Cui, C. Ge, Z. Xing, A. M. Asiri and X. Sun, *Electrochim. Acta*, 2014, **137**, 504-510.
7 T.-W. Lin, C.-J. Liu and J.-Y. Lin, *Appl. Catal.,B*, 2013, **134-135**, 75-82.
8 M. T. Koper and E. Bouwman, *Angew. Chem. Int. Ed.*, 2010, **49**, 3723-3725.
9 L. Liao, J. Zhu, X. Bian, L. Zhu, M. D. Scanlon, H. H. Girault and B. Liu, *Adv. Funct. Mater.*, 2013, **23**, 5326-5333.
10 D. Voiry, H. Yamaguchi, J. Li, R. Silva, D. C. B. Alves, T. Fujita, M. Chen, T. Asefa, V. B. Shenoy, G. Eda and M. Chhowalla, *Nat. Mater.*, 2013, **12**, 850-855.
11 Y. Zheng, Y. Jiao, M. Jaroniec and S. Z. Qiao, *Angew. Chem. Int. Ed.*, 2015, **54**, 52-65.
12 Y. Hou, B. L. Abrams, P. C. K. Vesborg, M. E. Björketun, K. Herbst, L. Bech, A. M. Setti, C. D. Damsgaard, T. Pedersen, O. Hansen, J. Rossmeisl, S. Dahl, J. K. Nørskov and I. Chorkendorff, *Nat. Mater.*, 2011, **10**, 434-438.
13 F. Harnisch, U. Schröder, M. Quaas and F. Scholz, *Appl. Catal. , B*, 2009, **87**, 63-69.
14 F. Harnisch, G. Sievers and U. Schröder, *Appl. Catal. , B*, 2009, **89**, 455-458.
15 J. Greeley, T. F. Jaramillo, J. Bonde, I. Chorkendorff and J. K. Norskov, *Nat. Mater.*, 2006, **5**, 909-913.
16 C. Lupi, A. Dell'Era and M. Pasquali, *Int. J. Hydrog. Energy*, 2009, **34**, 2101-2106.
17 S. Cobo, J. Heidkamp, P.-A. Jacques, J. Fize, V. Fourmond, L. Guetaz, B. Jousselme, V. Ivanova, H. Dau and S. Palacin, *Nat. Mater.*, 2012, **11**, 802-807.
18 J. Kibsgaard, T. F. Jaramillo and F. Besenbacher, *Nat. Chem.*, 2014, **6**, 248-253.
19 T. F. Jaramillo, K. P. Jørgensen, J. Bonde, J. H. Nielsen, S. Horch and I. Chorkendorff, *Science*, 2007, **317**, 100-102.
20 Y. Shi, J. K. Huang, L. Jin, Y. T. Hsu, S. F. Yu, L. J. Li and H. Y. Yang, *Sci Rep*, 2013, **3**, 1839.
21 D. Y. Chung, S. K. Park, Y. H. Chung, S. H. Yu, D. H. Lim, N. Jung, H. C. Ham, H. Y. Park, Y. Piao, S. J. Yoo and Y. E. Sung, *Nanoscale*, 2014, **6**, 2131-2136.
22 Z. Wu, B. Fang, A. Bonakdarpour, A. Sun, D. P. Wilkinson and D. Wang, *Appl. Catal. , B*, 2012, **125**, 59-66.
23 J. Yang, D. Voiry, S. J. Ahn, D. Kang, A. Y. Kim, M. Chhowalla and H. S. Shin, *Angew. Chem. Int. Ed.*, 2013, **52**, 13751-13754.
24 H. Zhang, Y. Li, G. Zhang, P. Wan, T. Xu, X. Wu and X. Sun, *Electrochim. Acta*, 2014, **148**, 170-174.
25 D. Kong, H. Wang, Z. Lu and Y. Cui, *J. Am. Chem. Soc.*, 2014, **136**, 4897-4900.
26 H. Zhang, B. Yang, X. Wu, Z. Li, L. Lei and X. Zhang, *ACS Appl. Mater. Interfaces*, 2015, **7**, 1772-1779.
27 M. S. Faber, R. Dziedzic, M. A. Lukowski, N. S. Kaiser, Q. Ding and S. Jin, *J. Am. Chem. Soc.*, 2014, **136**, 10053-10061.
28 M. R. Gao, Y. F. Xu, J. Jiang, Y. R. Zheng and S. H. Yu, *J. Am. Chem. Soc.*, 2012, **134**, 2930-2933.
29 M. R. Gao, J. X. Liang, Y. R. Zheng, Y. F. Xu, J. Jiang, Q. Gao, J. Li and S. H. Yu, *Nat. Commun.*, 2015, **6**, 5982.
30 Y. F. Xu, M. R. Gao, Y. R. Zheng, J. Jiang and S. H. Yu, *Angew. Chem. Int. Ed.*, 2013, **52**, 8546-8550.
31 K. Xu, F. Wang, Z. Wang, X. Zhan, Q. Wang, Z. Cheng, M. Safdar and J. He, *ACS Nano*, 2014, **8**, 8468-8476.
32 Q. Gong, L. Cheng, C. Liu, M. Zhang, Q. Feng, H. Ye, M. Zeng, L. Xie, Z. Liu and Y. Li, *ACS Catal.*, 2015, **5**, 2213-2219.
33 X. Zhan, Z. Wang, F. Wang, Z. Cheng, K. Xu, Q. Wang, M. Safdar and J. He, *Appl. Phys. Lett.*, 2014, **105**, 153903.
34 Z. Xing, Q. Liu, A. M. Asiri and X. Sun, *Adv. Mater.*, 2014, **26**, 5702-5707.
35 A. I. Carim, F. H. Saadi, M. P. Soriaga and N. S. Lewis, *J. Mater. Chem. A,* 2014, **2**, 13835-13839.
36 J. Xie, J. Zhang, S. Li, F. Grote, X. Zhang, H. Zhang, R. Wang and B. P. Yong Lei, † and Yi Xie* , †, *J. Am. Chem. Soc.*, 2013, **135**, 17881-17888.
37 J. Suntivich, K. J. May, H. A. Gasteiger, J. B. Goodenough and Y. Shao-Horn, *Science*, 2011, **334**, 1383-1385.
38 D. Kong, J. J. Cha, H. Wang, H. R. Lee and Y. Cui, *Energy Environ. Sci.*, 2013, **6**, 3553.
39 C. Xu, S. Peng, C. Tan, H. Ang, H. Tan, H. Zhang and Q. Yan, *J. Mater. Chem. A*, 2014, **2**, 5597-5601.
40 B. Losiewicz, *Int. J. Hydrog. Energy*, 2004, **29**, 145-157.

View Article Online
DOI: 10.1039/C5NR07735D

Table of contents:

Homogeneous $CoS_{2x}Se_{2(1-x)}$ (x ≈ 0.67) nanowires (NWs) arrays demonstrate excellent catalytic activity for electrochemical hydrogen evolution in acidic media, achieving current densities of 10 mA/cm^{2}and 100 mA/cm^2 at overpotentials of 129.5 mV and 174 mV, respectively.